The Meteoritical Society

Meteoritics & Planetary Science 50, Nr 8, 1362–1377 (2015)
doi: 10.1111/maps.12471

Opal-A in the Nakhla meteorite: A tracer of ephemeral liquid water in the Amazonian crust of Mars

M. R. LEE[1*], I. MACLAREN[2], S. M. L. ANDERSSON[2], A. KOVÁCS[3], T. TOMKINSON[1,4], D. F. MARK[4], and C. L. SMITH[5]

[1]School of Geographical and Earth Sciences, University of Glasgow, Glasgow G12 8QQ, UK
[2]SUPA School of Physics and Astronomy, University of Glasgow, Glasgow G12 8QQ, UK
[3]Ernst Ruska-Centrum für Mikroskopie und Spektroskopie mit Elektronen, Forschungszentrum Jülich GmbH, 52425 Jülich, Germany
[4]Scottish Universities Environmental Research Centre, East Kilbride G75 0QF, UK
[5]Department of Earth Sciences, Natural History Museum, London SW7 5DB, UK
[*]Corresponding author. E-mail: martin.lee@glasgow.ac.uk

(Received 23 February 2015; revision accepted 05 May 2015)

Abstract–The nakhlite meteorites are clinopyroxenites that are derived from a ~1300 million year old sill or lava flow on Mars. Most members of the group contain veins of iddingsite whose main component is a fine-grained and hydrous Fe- and Mg-rich silicate. Siderite is present in the majority of veins, where it straddles or cross-cuts the Fe-Mg silicate. This carbonate also contains patches of ferric (oxy)hydroxide. Despite 40 years of investigation, the mineralogy and origins of the Fe-Mg silicate is poorly understood, as is the paragenesis of the iddingsite veins. Nanometer-scale analysis of Fe-Mg silicate in the Nakhla meteorite by electron and X-ray imaging and spectroscopy reveals that its principal constituents are nanoparticles of opal-A. This hydrous and amorphous phase precipitated from acidic solutions that had become supersaturated with respect to silica by dissolution of olivine. Each opal-A nanoparticle is enclosed within a ferrihydrite shell that formed by oxidation of iron that had also been liberated from the olivine. Siderite crystallized subsequently and from solutions that were alkaline and reducing, and replaced both the nanoparticles and olivine. The fluids that formed both the opal-A/ferrihydrite and the siderite were sourced from one or more reservoirs in contact with the Martian atmosphere. The last event recorded by the veins was alteration of the carbonate to a ferric (oxy)hydroxide that probably took place on Mars, although a terrestrial origin remains possible. These results support findings from orbiter- and rover-based spectroscopy that opaline silica was a common product of aqueous alteration of the Martian crust.

INTRODUCTION

A proportion of the meteorites in our collections that are from Mars contain minerals that precipitated from liquid water. These rocks can therefore provide very valuable information on the Martian hydrosphere, including its temperature, elemental composition, pH, Eh (i.e., redox potential), and longevity (e.g., Ashworth and Hutchison 1975; Treiman et al. 1993; Treiman and Lindstrom 1997; Bridges and Schwenzer 2012; Tomkinson et al. 2013). The nakhlites are cumulate clinopyroxenites, most of which are olivine-bearing, and contain the greatest volume and diversity of water-formed minerals among the Martian meteorites. Collectively called "iddingsite," these minerals include phyllosilicates, carbonates, sulfates, and halides (e.g., Bunch and Reid 1975; Reid and Bunch 1975; Gooding et al. 1991; Treiman et al. 1993; Bridges and Grady 2000; Noguchi et al. 2009; Changela and Bridges 2011; Lee et al. 2013, 2015; Tomkinson et al. 2013, 2015). A preterrestrial (i.e., Martian) origin for the iddingsite is demonstrated by the fact that it is cut by the meteorite

Table 1. Chemical compositions of Fe-Mg silicate in the nakhlites.

	Nakhla[a]	NWA 998[b]	MIL 03346[c]	Lafayette[d]	NWA 817[e]	Y-000593[f]	Y-000749[f]
SiO_2	40.2	37.44	44.98	48.40	42.82	51.35	50.12
TiO_2	0.02	0.06	0.05	0.01	0.06	bd	bd
Al_2O_3	0.74	1.02	0.22	4.19	0.21	0.56	0.41
Cr_2O_3	0.03	0.00	0.05	0.00	0.03	bd	bd
Fe_2O_3	37.9	43.96	40.63	30.56	40.41	28.44	30.87
NiO	<0.01	—	—	0.09	—	bd	bd
MnO	0.63	0.81	0.65	0.48	0.55	0.22	0.24
MgO	6.82	4.14	3.10	13.61	5.69	3.80	3.55
CaO	1.14	3.04	0.07	0.71	0.25	0.08	0.14
Na_2O	1.16	0.05	—	0.31	0.18	bd	0.14
K_2O	0.60	0.49	—	0.35	0.41	0.52	0.51
P_2O_5	0.06	—	—	0.09	—	—	0.14
SO_3	0.14	—	—	0.80	—	2.79	1.75
Cl	0.66	—	—	0.41	—	—	—
Total	90.1	91.00	89.75	100.00	90.61	87.76	87.87

[a]Gooding et al. (1991). Mean of 78 analyses by SEM-EDX.
[b]Treiman and Irving (2008). Mean of three electron probe analyses.
[c]Day et al. (2006). Mean of four electron probe analyses.
[d]Treiman et al. (1993). Mean of two sets of normalized analyses of "fine phyllosilicate" by TEM-EDX. Fifty-three analyses in total.
[e]Gillet et al. (2002). Mean of 25 electron probe analyses.
[f]Noguchi et al. (2009) electron probe data.
— denotes not analyzed for. bd denotes below detection limits.

fusion crust (Gooding et al. 1991), and samples from the Lafayette and Yamato-000593 meteorites yield a radiometric formation age of 633 ± 23 Ma (i.e., Amazonian: Borg and Drake 2005). The eight nakhlites have a common age of crystallization (Amazonian, 1327 ± 39 Ma; Borg and Drake 2005) and impact ejection (~11 Ma; Eugster et al. 1997), which together with petrologic and compositional similarities suggests that they were derived from the same igneous body, probably a lava flow or shallow sill (Friedman-Lentz et al. 1999; Mikouchi et al. 2006, 2012).

The component of iddingsite that is most widespread among the nakhlites has been difficult to identify. X-ray microanalysis shows that it is rich in O, Mg, Si, and Fe, and analytical totals of ~90 wt% suggest that it contains water (Table 1). This inference of a hydrous composition is supported by the detection of H by ion microprobe (Hallis et al. 2012); therefore, this material is the main carrier of Martian water that is available for examination in terrestrial laboratories. For brevity, we refer to it as the "Fe-Mg silicate," although we show later that it is not a single mineral as this term may suggest. The first attempt to identify the Fe-Mg silicate was in a study of Nakhla by Ashworth and Hutchison (1975). Using transmission electron microscopy (TEM), they found that it ranges in microstructure from fine-grained to "colloidal." Their selected area electron diffraction (SAED) patterns contained rings, thus indicating that it has a finely crystalline constituent. However, despite being the subject of a series of investigations over the intervening 39 yr, there is still no consensus regarding the mineralogy of the Fe-Mg silicate, or even its crystallinity (Tables 2 and 3).

Table 2. Previously identified constituents of Nakhla Fe-Mg silicate.

Constituent(s) identified	Technique
Fine-grained/colloidal material[a]	TEM
Nanophase goethite[b]	Mössbauer
Smectite[c]	EPMA; TEM
Iron saponite, iron-bearing smectite, serpentine, hematite, two-ring ferrihydrite[d]	TEM
Smectite, hematite, goethite, quartz, cristobalite, tridymite, amorphous silica[e]	TEM
Smectite/illite, goethite[f]	EPMA
Amorphous gel[g]	TEM
Smectite[h]	TEM

[a]Ashworth and Hutchison (1975).
[b]Burns (1991), Burns and Martinez (1990).
[c]Gooding et al. (1991).
[d]Treiman and Gooding (1991).
[e]Thomas-Keprta et al. (2000).
[f]Bridges and Grady (2000).
[g]Changela and Bridges (2011), Hicks et al. (2014).
[h]Lee et al. (2013).
EPMA = electron probe microanalysis.

Table 3. Previously identified constituents of Fe-Mg silicate in nakhlites other than Nakhla.

Meteorite	Constituent(s) identified	Technique
Lafayette[a]	Ferrous saponite, ferrihydrite, magnetite	TEM
Lafayette[b]	Two-ring ferrihydrite	Not stated
MIL 03346[c]	Smectite	EPMA
MIL 03346[d]	Serpentine and saponite	EMPA
MIL 03346[e]	Stilpnomelane, hematite	Raman, EPMA
MIL 03346[f]	Fe-smectite	TEM
NWA 817[g]	Fe-smectite	XRD, TEM, Raman, EPMA
Y-000749[h]	Iddingsite (30% goethite + 70% montmorillonite)	FTIR
Y-000749[i]	X-ray amorphous material, smectite, Fe-oxyhydroxide	S-XRD
Y-000593 & -000749[j]	Smectite, Fe-hydroxides, serpentine	TEM
All nakhlites except NWA 5790[k]	Amorphous gel	TEM

[a]Treiman et al. (1993).
[b]Treiman (2009).
[c]Sautter et al. (2006).
[d]Imae and Ikeda (2007).
[e]Kuebler (2013).
[f]Hallis et al. (2014).
[g]Gillet et al. (2002).
[h]Imae et al. (2003).
[i]Treiman et al. (2004).
[j]Noguchi et al. (2009).
[k]Changela and Bridges (2011).
FTIR = Fourier transform infrared spectroscopy; Raman = Raman spectroscopy; XRD = X-ray diffraction; S-XRD = Synchrotron X-ray microdiffraction.

The fine grain size of the Fe-Mg silicate is likely to be one of the main reasons why it has been so hard to characterize. Its hydrous composition may also exacerbate the problem by rendering samples susceptible to damage during analysis by ion- and electron-beam methods. Therefore, we have sought to identify the constituent(s) of the Fe-Mg silicate using imaging and spectroscopy techniques that are appropriate for studying beam-sensitive materials at high spatial resolutions. We have also investigated the other components of the iddingsite veins in the hope that they can shed further light on the origin of the Fe-Mg silicate. Our work has focused on Nakhla because it is the same meteorite that was first studied by Ashworth and Hutchison (1975). In addition, as it is the only confirmed fall among the nakhlites, it is likely to have undergone little terrestrial weathering. Thus, any constituents of the Fe-Mg silicate that are identified can be used with confidence to explore aqueous environments within the Amazonian crust of Mars.

MATERIALS AND METHODS

The Nakhla Sample

Nakhla was recovered in 1911, shortly after it was seen to fall near to the village of El Nakhla El Baharia in Egypt (Prior 1912). This meteorite contains augite (79.4 vol.%), olivine (9.5 vol%), and an intercumulate mesostasis (11.1 vol.%) (Needham et al. 2013). Iddingsite veins comprise ~1 wt% of the rock, and are assumed to be the host to most of the meteorite's 0.11–0.13 wt% water (Karlsson et al. 1992; Leshin et al. 1996). We studied two samples of Nakhla that were loaned by Natural History Museum (London): a petrographic thin section (BM1913,026 #2) and a 1.7 g chip of BM1913, 25. Subsamples of the chip were impregnated in epoxy resin then polished and carbon coated.

Scanning and Transmission Electron Microscopy

Iddingsite veins were located by backscattered electron (BSE) imaging using a FEI Quanta 200F field-emission SEM operated at 20 kV. Electron-transparent foils were extracted from the veins and their host olivine grains using the focused ion beam (FIB) liftout method (Lee et al. 2003) employing a FEI Nova Nanolab 200 dual-beam instrument; initial milling used 30 kV Ga^+ ions, with final polishing at less than 10 kV. To ensure that damage to the sidewalls of the foil by the Ga^+ ions had been effectively removed, final thinning was undertaken by argon ion milling using a Fischione Nanomill operated at 500 eV for 20 min on either side of the foil. As one or more of the components of the iddingsite are potentially electron beam-sensitive, we have taken great care during TEM work to minimize the potential for damage, which can be recognized by amorphization and migration of ions (e.g., Lee et al. 2007). Bright- and dark-field TEM images and SAED patterns of the foils were obtained using a FEI Tecnai T20 TEM operated at 80 kV; the selected aperture used to obtain the diffraction patterns was 100 nm in diameter. Further investigation of nanoscale chemistry was performed by scanning TEM (STEM) using a JEOL ARM200F. The instrument was operated at either 80 or 200 keV with a beam current ~100 pA, and has a nominal spot size in STEM mode of <0.2 nm. The ARM200F was used for high angle annular dark-field (HAADF) imaging, electron energy loss spectroscopy (EELS) employing a Gatan GIF Quantum

ER electron energy loss spectrometer, and energy-dispersive X-ray (EDX) analysis via a Bruker 60 mm^2 SDDEDX spectrometer. The EELS and EDX data were acquired simultaneously, and maps were recorded with spatial resolutions down to 1 nm. STEM imaging of foils postanalysis revealed no detectable beam damage, although a slight shrinkage of the Fe-Mg silicate was observed, suggesting a minor loss of water in the vacuum environment.

Processing of EELS and EDX Data Sets

Dual EELS data sets were first treated by aligning all pixels to the same energy scale using the zero loss peak as a constant reference. These data sets were then trimmed of the noisy pixels at the two extreme ends of the spectra. Principal component analysis (PCA) was performed using the package of Lucas et al. (2013) to separate the real spectroscopic signals from random noise components in the data sets. Quantification of the data to provide elemental concentrations was performed using a new EELS modeling package (Elemental Quantification for Gatan Microscopy Suite 2.3) which takes into account multiple scattering using explicit consideration of the low loss in the quantification; the cross sections used in the calculation were determined using a standard Hartree–Slater method. EDX data sets were also processed via the application of PCA using the same plugin (Lucas et al. 2013) and were quantified using the Elemental Quantification plugin referred to above. The locations of different minerals were mapped using multiple linear least squares fitting (MLLS) treating the EELS data sets as a linear sum of simple spectra for each mineral. Valence state maps were calculated from suitable EELS data sets by background subtracting the Fe-$L_{2,3}$ edges from a data set, then by deconvolution of the low loss using the Fourier ratio method to remove the effects of multiple scattering. The resulting data sets were then fitted in the 705–720 eV energy range as a linear combination of a standard spectra for Fe^{2+} (FeO) and Fe^{3+} (Fe_2O_3), allowing an easy visualization of the spatial distribution of each valence state.

RESULTS

Petrographic Context of the Iddingsite Veins

Iddingsite veins are readily identifiable in thin section by their orange color in plane polarized transmitted light (Fig. 1a). They occur within all olivine grains, along olivine–augite grain boundaries, and rarely within augite (Figs. 1 and 2). The abundance of iddingsite within olivine grains ranges from 2.7 to 7.3 vol% (mean 4.3 vol%; $n = 990$ points in five grains). The majority of veins are only a few tens of micrometers in length, and almost all of these "discontinuous" veins occur at olivine grain boundaries (Fig. 1c). A small proportion of iddingsite veins cross-cut entire ~300–1000 μm-sized olivine grains. These veins are often widest in the vicinity of grain boundaries, and the mean width of individual veins ranges from 1.9 to 7.0 μm (mean 3.5 μm; $n = 14$ veins). The olivine walls of iddingsite veins may be straight or finely serrated (Fig. 1c), depending on their crystallographic orientation (Lee et al. 2013), and finer scale serrations are present on the walls of a small proportion of augite-hosted fractures (Fig. 1c). Three vein components have been identified, which in order of decreasing abundance are (1) Fe-Mg silicate, (2) siderite, and (3) ferric (oxy)hydroxide. Some veins contain only Fe-Mg silicate, but in most veins it is intergrown with either or both of the other two components (Figs. 2 and 3).

Constituents of the Fe-Mg Silicate

The Fe-Mg silicate may be internally featureless in BSE images (Fig. 2a), or can have a submicrometer wide axial layer that is distinguished from flanking layers by a difference in mean atomic number (Z) (Fig. 2b). STEM-EDX analysis of FIB-produced foils shows that the Fe-Mg silicate is rich in O, Mg, Si, and Fe, with detectable Cl and K (Table 4), and this composition agrees with previous analyses of Nakhla veins in thin section (Table 1). EELS point analyses and maps show that the iron is dominantly ferric (Fig. 3), which is consistent with the orange color of the iddingsite veins in transmitted light (Ashworth and Hutchison 1975; Bunch and Reid 1975) (Fig. 1a).

The Fe-Mg silicate is almost featureless in bright-field TEM images (Fig. 3a), but HAADF reveals that it is composed of closely packed particles that are circular to oval in shape (Fig. 4a). These particles have a common structure comprising a core and a shell. The cores range in diameter from 5 nm to 29 nm (mean 12 nm; $n = 18$) and have a relatively low scattering intensity (corresponding to a relatively low Z), whereas the shells have a substantially higher Z (Figs. 4a and 4b). EDX and EELS maps confirm that the HAADF contrast corresponds to differences in elemental composition; relative to their cores the nanoparticle shells are depleted in Si and enriched in Mg and Fe^{3+}. Oxygen is present in both the cores and shells (Fig. 4b). Based on X-ray spectra from one of the largest cores, they are almost pure silica (Fig. 5a), and the broad diffuse ring in SAED patterns obtained from groups of nanoparticles shows that the majority of them are

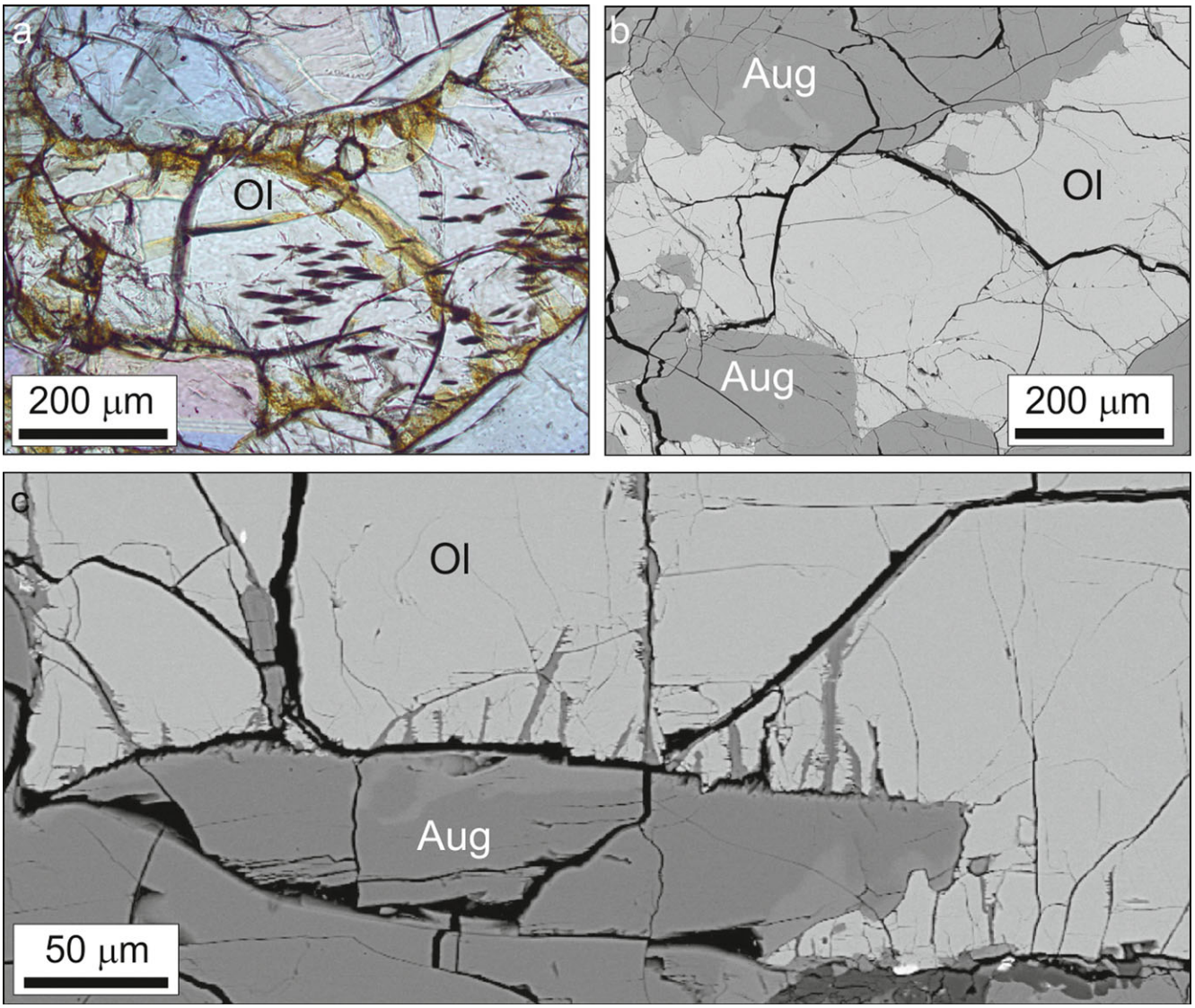

Fig. 1. Images of iddingsite veins in olivine (Ol) grains from the Nakhla thin section. a) Plane polarized transmitted light image of an olivine grain that is cross-cut by veins (orange). The small black oval shaped inclusions in the center of the image are symplectites. b) BSE image of the same field of view as (a). The olivine is surrounded by augite (Aug). c) BSE image of the edge of an olivine grain that is in contact with augite (Aug). Discontinuous veins of iddingsite (mid gray) are abundant within olivine and close to the intergranular boundary, but few of them extend further into olivine, and none occur within augite.

amorphous (Fig. 5b). This finding is supported by the absence of reflections in SAED patterns with d-spacings attributable to crystalline silica (e.g., cristobalite, trydimite, quartz). Given that bulk Fe-Mg silicate contains ~10 wt% water, the silica is most probably opal-A (amorphous $SiO_2 \cdot nH_2O$).

The d-spacings of the continuous narrow rings in SAED patterns are consistent with two-line ferrihydrite (e.g., Janney et al. 2000) (Fig. 5b), whose formula is $Fe_{8.2}O_{8.5}(OH)_{7.4} + 3H_2O$ (Michel et al. 2010). Therefore, this mineral is host to a portion of the water held within the bulk Fe-Mg silicate. Dark-field TEM images that were acquired using different parts of one of the diffraction rings show that these ferrihydrite crystals range in size from 3 nm to 21 nm (mean 6 nm; $n = 18$) and are dispersed fairly uniformly throughout the Fe-Mg silicate (Fig. 5c). Such a size and distribution suggests that ferrihydrite crystals occur mainly in the high Z- and Fe^{3+}-rich nanoparticle shells.

Siderite and Ferric (oxy)Hydroxide

The siderite has a composition of ~$Fe_{0.54}Mg_{0.40}Ca_{0.06}CO_3$ (Table 5), and typically forms a ~1 μm wide band between olivine and the Fe-Mg silicate (Figs. 2 and 3). These bands have a sharp

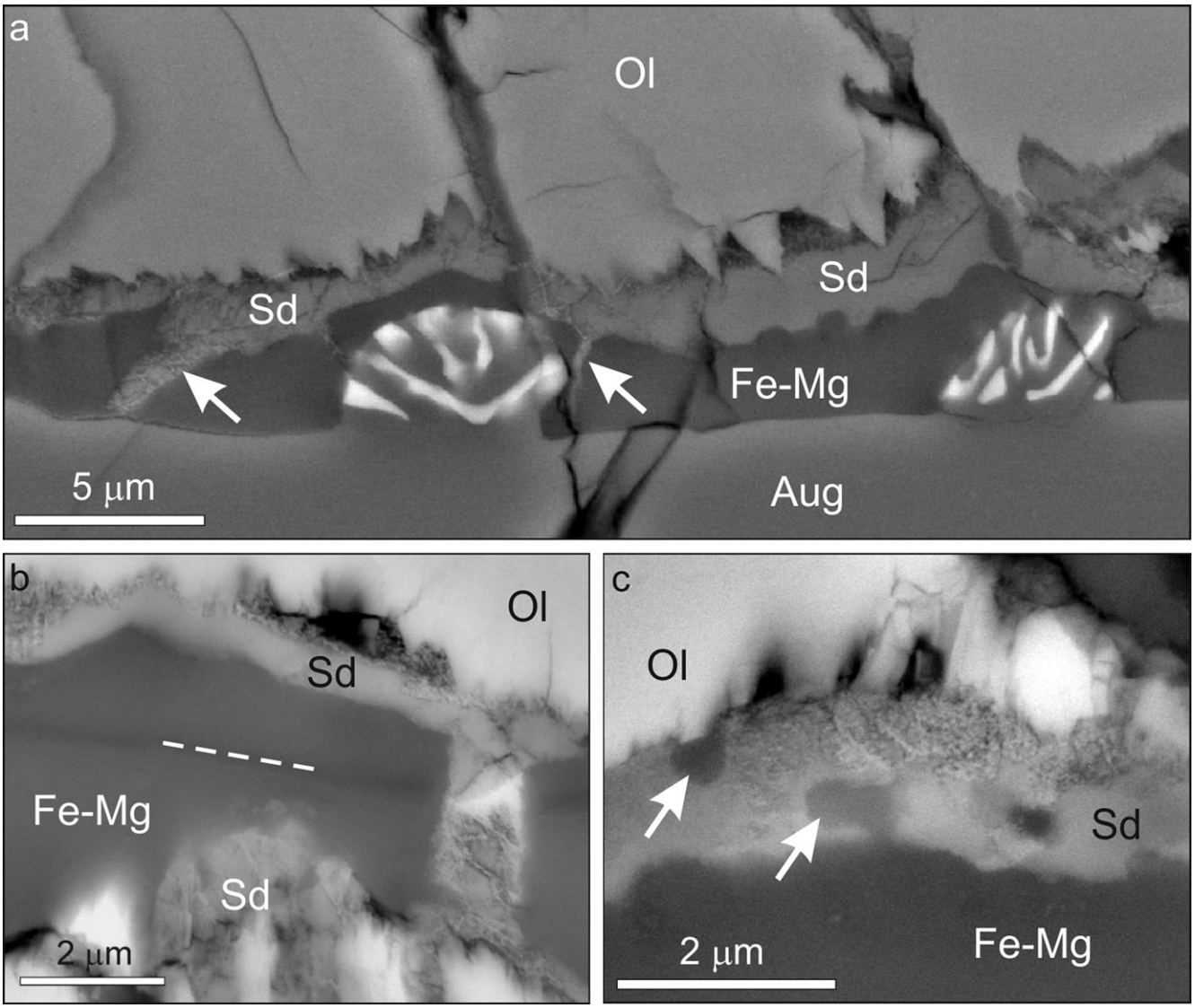

Fig. 2. BSE images of iddingsite veins within grains of olivine (Ol). The veins contain Fe-Mg silicate (Fe-Mg) and siderite (Sd). a) A vein at the interface between olivine and augite (Aug) that contains Fe-Mg silicate and siderite. Siderite lines the serrated olivine vein wall, and cross-cuts the Fe-Mg silicate in several places (indicated by arrows). The interface between siderite and Fe-Mg silicate is finely corrugated. Two symplectites (intergrowths of augite [gray] with magnetite [white]) are in contact with the augite grain boundary. b) A vein whose Fe-Mg silicate has an axial band, which is highlighted by a dashed white line along part of its length. The axial band is cross-cut by a strip of siderite. This siderite has been partially altered to patches and lamellae of a material with a substantially higher mean atomic number (white in the image). c) A vein containing siderite that hosts rounded inclusions of the Fe-Mg silicate (arrowed). a) is from a polished chip, whereas b) and c) are from the thin section.

contact with olivine so that siderite fills notches in the serrated vein walls (Fig. 2a). The interface between siderite and Fe-Mg silicate may be straight or corrugated (Fig. 2), and where corrugations are strongly developed the Fe-Mg silicate occupies lobate depressions in the edge of the carbonate. Fe-Mg silicate may also occur as rounded inclusions within the siderite (Fig. 2c). Parallel-sided strips of siderite that are ~1 μm in width partially or completely cross-cut the Fe-Mg silicate (Figs. 2a and 2b).

The siderite often contains irregular patches or lamellae of a very fine-grained material that relative to its host carbonate is enriched in O and Fe, and depleted in C (Table 5). Veinlets of this material may also cross-cut the Fe-Mg silicate. A ternary plot of C, O, and (Ca+Mg+Fe) shows that the patches fall on a line between Nakhla siderite and ideal ferrihydrite and goethite (Fig. 6), thus indicating that the analyzed volume contains a mixture of carbonate and ferric (oxy)hydroxide. EELS confirms that a proportion of

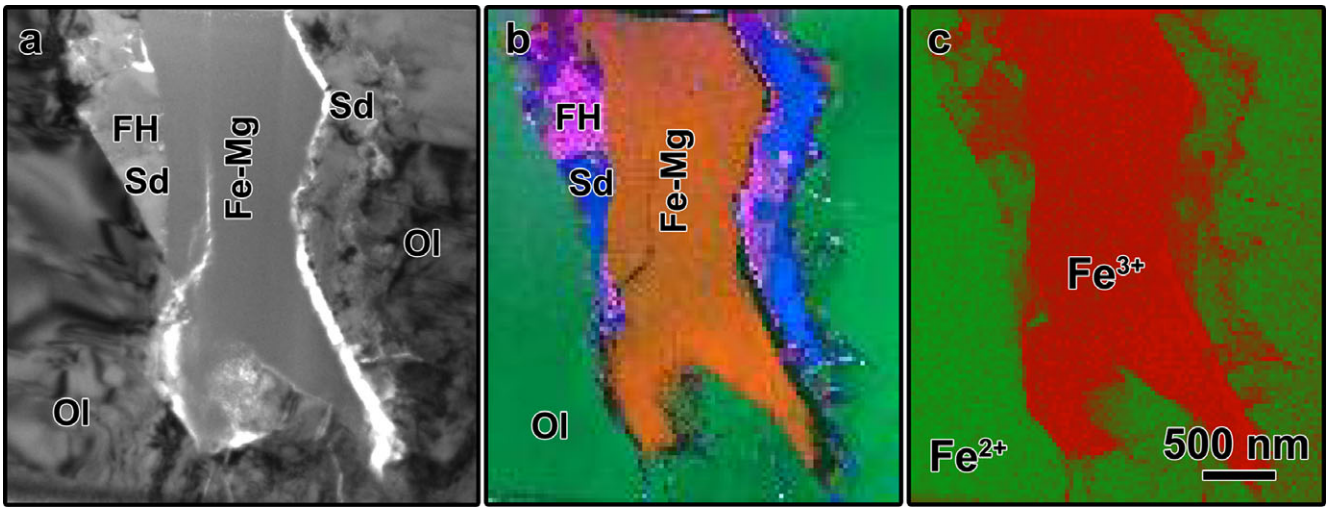

Fig. 3. (S)TEM images of a foil that was cut from an olivine (Ol) hosted iddingsite vein containing Fe-Mg silicate (Fe-Mg), siderite (Sd), and ferric (oxy)hydroxide (FH). a) Bright-field TEM image. b, c) Spectral maps generated from EELS spectrum images of (a). Spectral fingerprinting of different phases using multiple linear least squares fitting in (b) reveals the distribution within the foil of olivine (green), siderite (blue), Fe-Mg silicate (orange), and ferric (oxy)hydroxide (pink). A map of Fe oxidation states in (c) shows that the olivine and siderite contain Fe^{2+} (green), whereas the Fe-Mg silicate and ferric (oxy)hydroxide patches both contain Fe^{3+} (red).

Table 4. Chemical composition of the Nakhla Fe-Mg silicate.

Compound (X-ray line)	wt%
SiO_2 (from Si-K_α)	40.2
Fe_2O_3 (from Fe-K_α)	36.3
MgO (from Mg-K_α)	10.2
K_2O (from K-K_α)	1.4
Cl (from Cl-K_α)	1.1
H_2O (assumed from excess O, from O-K_α)	10.8

Data obtained by STEM-EDX. Statistical errors are minimal at less than 1% in all cases. Quantification was performed using calculated k-factors without standards, and there could be some smaller systematic errors, although large errors are not expected for K_α-peaks. O and thus H_2O could be underestimated due to the absorption of the low energy O-K_α X-rays in the sample and water loss in the vacuum.

iron in these patches is ferric (Fig. 3c), and hereafter this material is referred to as "ferric (oxy)hydroxide" to distinguish it from ferrihydrite in the nanoparticle shells. Note that although ferric oxides and (oxy)hydroxides have been described from Nakhla (Table 2), in most cases the context of these minerals (i.e., whether they occur within the Fe-Mg silicate or siderite) was not stated.

DISCUSSION

Here, we interpret and discuss our observations regarding the nature and sequence of formation of the three vein components, develop a model for precipitation of the Nakhla iddingsite in the context of an Amazonian fluid system, and explore the implications of our findings for understanding water–rock interaction on Mars.

Creation of Space for the Veins

Space for the iddingsite veins is inferred to have been created primarily by the dissolution of olivine rather than by opening of fractures. The principal evidence for this conclusion is the presence of fine-scale serrations on vein walls, which are comparable in size and shape to etch pits in weathered terrestrial olivine (Velbel 2009; Lee et al. 2013). The finding that veins decrease in abundance and become narrower away from grain boundaries is also consistent with their formation by reaction of olivine with aqueous solutions (i.e., because these solutions must have been sourced from outside of the olivine grains). Furthermore, Lee et al. (2013) found that olivine-hosted iddingsite veins straddle the lamellar symplectites and do not cross-cut them, which can be best accounted for if the veins formed by dissolution in the presence of solutions whose composition was such that olivine was more soluble than the augite–magnetite intergrowths.

Sequence of Formation of the Three Iddingsite Components

The two main iddingsite components (i.e., Fe-Mg silicate and siderite) could have formed by one of two

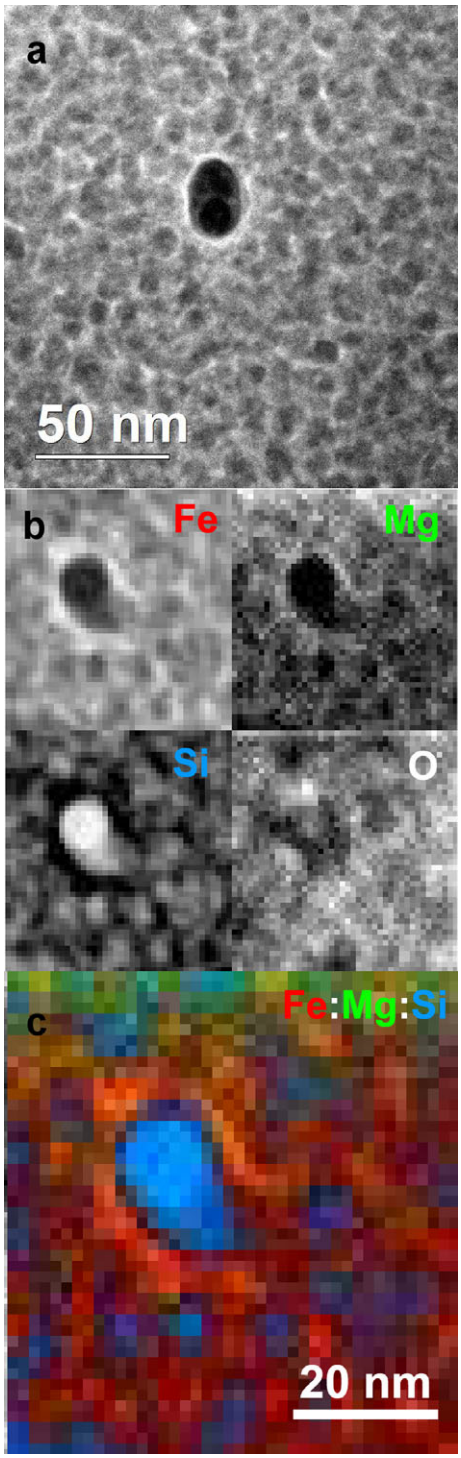

Fig. 4. Nanostructural details of the Fe-Mg silicate. a) HAADF STEM image of the nanoparticles. The shells have the highest average Z and are white. b and c) Elemental maps created from EELS spectrum imaging showing the distribution of O, Mg, Si, and Fe.

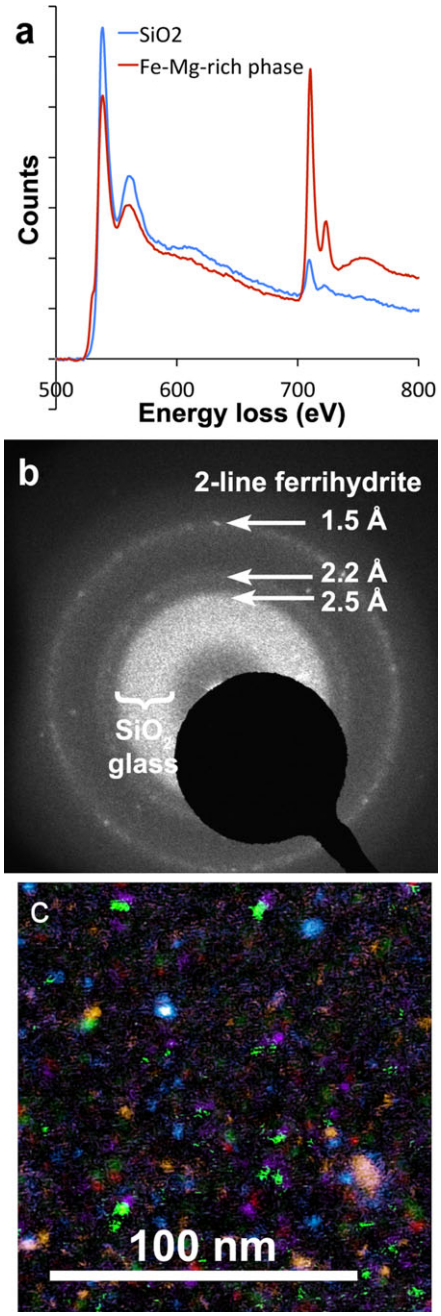

Fig. 5. a) EELS spectra from a relatively large silica nanoparticle (blue) and from its shell (red), concentrating on the region around the O-K edge at ~532 eV and the Fe-$L_{2,3}$ edge around 708 eV. b) SAED pattern from a group of nanoparticles showing features consistent with a mixture of two-line ferrihydrite and amorphous silica (labeled SiO_2 glass). c) A composite of several dark-field TEM images of Fe-Mg silicate produced using the 2.2 Å diffraction ring, which shows that the ring has been formed by scattering from many ferrihydrite nanocrystals.

processes (1) partial cementation by siderite of pores that had been produced by the congruent dissolution of olivine, then later occlusion of the remaining space by Fe-Mg silicate or (2) formation of Fe-Mg silicate veins, then precipitation of siderite by replacement of olivine and/or the Fe-Mg silicate. The first process can only

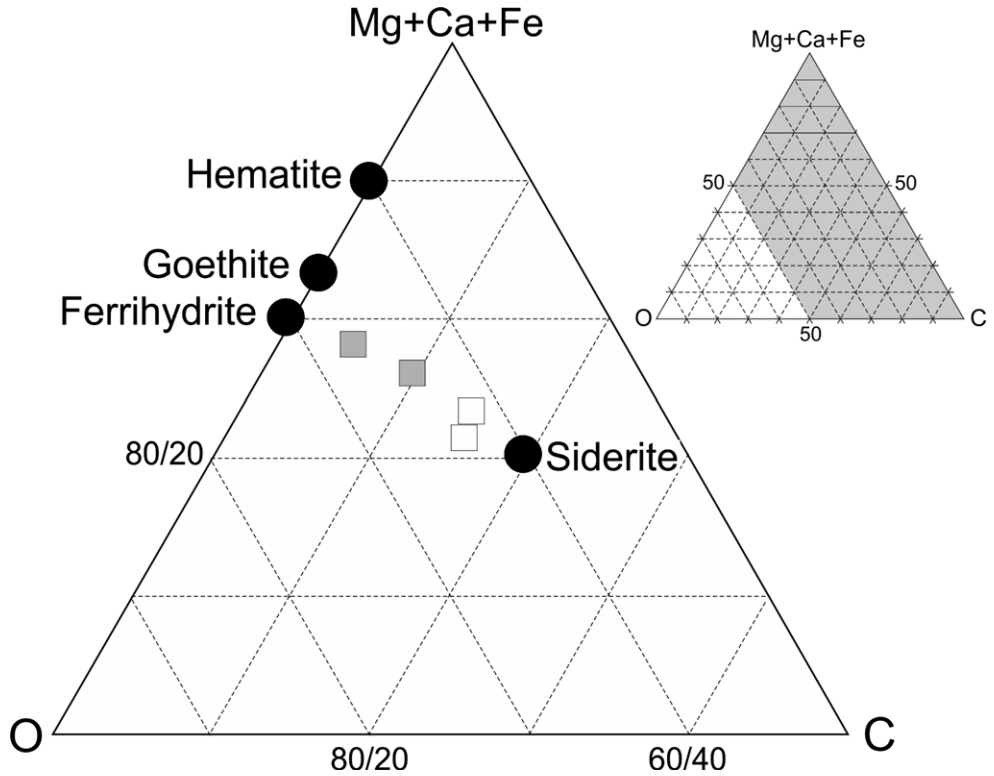

Fig. 6. Ternary diagram showing the chemical composition of Nakhla siderite (white squares) and ferric (oxy)hydroxide patches (gray squares). The data are expressed in atomic proportions and were acquired by STEM-EDX. Values are listed in Table 5. The ideal compositions of siderite and various Fe-oxides/(oxy)hydroxides are included for reference (black circles).

Table 5. Chemical compositions of Nakhla olivine, siderite, and ferric (oxy)hydroxide.

	Olivine	Siderite	Siderite	Ferric (oxy)hydroxide	Ferric (oxy)hydroxide
Si	13.6	bd	0.1	0.2	1.4
Fe	19.5	15.5	16.6	22.2	18.9
Mn	—	—	—	0.4	—
Mg	8.9	4.8	5.5	4.3	5.5
Ca	—	1.1	1.4	1.0	1.0
Na	—	—	—	1.6	0.8
K	—	bd	bd.	0.1	—
Cl		bd	bd	0.3	0.2
O	58.0	63.1	62.1	65.7	63.3
C	—	15.6	14.2	4.3	10.5

Data obtained by STEM-EDX. Values in atom%, normalized to 100 wt%. bd denotes below detection limits. — denotes not analyzed for.

account for the strips of siderite that project into or cross-cut Fe-Mg silicate if carbonate crystals had grown as a meshwork within pre-existing pores. However, given that siderite crystals typically have low aspect ratio habits, it is more likely that they would have grown as equant cements than a meshwork. The second process readily accounts for the rounded inclusions of Fe-Mg silicate within carbonate (i.e., these inclusions are pieces of Fe-Mg silicate that were preserved as siderite grew around them, and the corrugated interface between siderite and Fe-Mg silicate confirms that the replacement front was irregular). The parallel-sided strips of siderite could therefore have formed by fracture-guided replacement of the Fe-Mg silicate. Further evidence in support of this process comes from distinct similarities in petrographic relationships between olivine, siderite, and Fe-Mg silicate in Nakhla, and olivine, carbonate (calcite), and serpentine in peridotites from Oman. In these terrestrial samples, Hövelmann et al. (2011, p. 6775) noted that "the primary olivine has been directly replaced by calcite along the contact with the surrounding serpentine. The calcite forms a continuous rim around the remnant olivine while the interface is saw-toothed and decorated with pores." Thus, although fluid conditions are likely to have been quite different between Oman and the nakhlites, this comparison demonstrates that carbonates can form by replacement of the walls of hydrous silicate veins.

We conclude that veins of Fe-Mg silicate formed first, and then siderite grew by replacement. The petrographic context of the ferric (oxy)hydroxide (i.e.,

irregular patches and lamellae with siderite) indicates that it was the last of the three components, and formed by oxidation of the carbonate. This interpretation for the origin of the ferric (oxy)hydroxide agrees with previous reports of alteration of the Nakhla carbonates (Saxton et al. 2000; Chatzitheodoridis et al. 2014), and Treiman and Gooding (1991) likewise concluded that patches and veinlets of hematite and ferrihydrite were the last of the secondary minerals to have formed in Nakhla veins. The presence within ferric (oxy)hydroxide patches of Si, Cl, and K, which are otherwise absent from the siderite, shows that the fluid responsible for alteration of the carbonates had interacted with pre-existing Fe-Mg silicate, and so further supports the sequence of events outlined above.

Origin of the Fe-Mg Silicate

Our finding that opal-A is the principal constituent of the Fe-Mg silicate agrees with the discovery of silica in Nakhla iddingsite veins by Thomas-Keprta et al. (2000) (Table 2). Terrestrial opal varies considerably in its particle size (tens to thousands of nanometers) and shape (spheres, platelets, fibers) (Gaillou et al. 2008). The variety of opal that diffracts visible light to produce different colors (termed "play of color opal") is composed of spheres that are ~150–400 nm in diameter and packed in a regular three-dimensional array (Sanders 1964). Fe-Mg silicate in the Nakhla veins is much more similar to terrestrial "fire opal," which is typically orange in color and composed of particles of silica that are ~20 nm in size and randomly arranged (Fritsch et al. 2006). The color of fire opal is due to the presence of ferric oxides rather than diffraction (Fritsch et al. 2006). In addition to amorphous silica, Thomas-Keprta et al. (2000) found that Nakhla iddingsite contains three polymorphs of crystalline silica, namely cristobalite, trydimite, and quartz. On Earth, these polymorphs of silica commonly form by the water-mediated recrystallization of opal-A (Smith et al. 2013); where cristobalite and trydimite are the dominant constituents, the material is referred to as opal-CT.

Several of the previous TEM studies of Nakhla have found that its Fe-Mg silicate contains crystallites of smectite (primarily identified from their distinctive ~10–15 Å lattice fringe spacing in TEM images; Table 2). This clay mineral was not identified in the samples studied here, which could suggest that the mineralogy of the Fe-Mg silicate differs between samples of Nakhla. Alternatively, smectite may have been present in the nanoparticle shells but was not identified owing to our desire to minimize electron beam damage by limiting the amount of high-resolution imaging that was undertaken. The occurrence of smectite in the nanoparticle shells would be consistent with the curved and rounded shapes of individual clay mineral crystallites (Thomas-Keprta et al. 2000; Lee et al. 2013). Given that these shells are rich in ferric iron, this putative smectite could be nontronite, i.e., $(Ca_{0.5},Na)_{0.3}Fe^{3+}{}_2(Si,Al)_4O_{10}(OH)_2 \cdot nH_2O$. Smectite may therefore account for some or all of the Na, Al, and Ca that occurs within the bulk Fe-Mg silicate (Tables 1 and 4), whereas the Cl and K would more likely be associated with ferrihydrite given its significant capacity for sorption.

As Fe-Mg silicate was the first component of iddingsite to form, and space for it was created by dissolution, it is reasonable to assume that olivine was the principal source of silica for the opal-A. The almost exclusive occurrence of Fe-Mg silicate within olivine grains suggests that the silica was transported in solution over very short distances (i.e., tens to hundreds of micrometers at most). Such a local provenance for the silica indicates that dissolution of olivine and precipitation of opal-A was coupled at the water–mineral interface. This finding implies that the solubility of silica was very low, which in turn suggests that fluids were acidic to circumneutral (the solubility of silica is very low below pH 8 and increases abruptly in progressively more alkaline solutions; Alexander et al. 1954). Formation of the Fe-Mg silicate at low pH is also consistent with the presence in nanoparticle shells of ferrihydrite, and possibly also nontronite, because both minerals are stable in oxidizing and weakly acidic to neutral solutions that are saturated with respect to amorphous silica (Chevrier et al. 2007). The ferrihydrite is interpreted to have formed on Mars because Prior (1912) observed within ~6 months of the fall of Nakhla that its olivine grains were "reddish-brown," and this coloration is most likely due to the presence of ferric oxyhydroxides in the iddingsite veins. We acknowledge, however, the possibility that ferric oxyhydroxide formed by reaction of the nanoparticles with the Earth's atmosphere, especially as Hallis et al. (2012) demonstrated that terrestrial water has entered Nakhla iddingsite veins and lowered their original deuterium/hydrogen ratio.

These conclusions about the nature of the environment within which the opal-A formed enable further constraints to be placed on the properties of the aqueous solutions. As the Fe-Mg silicate has considerably lower Mg/Si and Fe/Si ratios than precursor olivine, Fe and Mg must have been leached from the veins relative to Si. Olivine and Fe-Mg silicate both have an atomic Fe/Mg ratio of 2 (Fig. 7), which means that the same proportion of these two ions was removed. This finding is surprising because Mg would

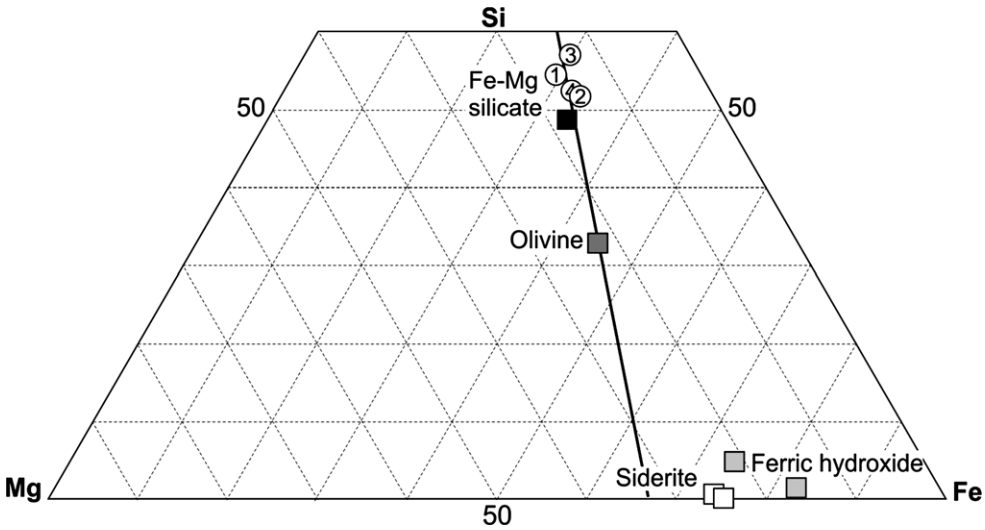

Fig. 7. Ternary diagram showing the chemical compositions of Nakhla olivine and the three iddingsite vein components (plotted using square symbols). The data, expressed in atomic proportions, were acquired by STEM-EDX and values are listed in Tables 1, 4, and 5. The solid line joins parts of the ternary diagram that have a Fe/Mg ratio of 2, which includes both the olivine and Fe-Mg silicate. Also plotted are the compositions of Nakhla Fe-Mg silicate as determined by analyses of veins in thin section: 1 = Bunch and Reid (1975); 2 = Gooding et al. (1991); 3 = Hallis et al. (2012); 4 = Lee et al. (2013).

be expected to be leached much more readily than Fe given the differences in the solubility of these two ions in oxidizing solutions (i.e., Fe^{2+} liberated from the olivine should have been quickly oxidized to much less soluble Fe^{3+}). The explanation for this apparent contradiction may lie in the pH dependence of the oxidation rate of Fe^{2+}. As oxidation rate is slowest at a pH of <~4 (Hurowitz et al. 2006), Fe^{2+} could have remained in solution within acidic fluids for a sufficient time to have been leached along with Mg. Elements that are present within the Fe-Mg silicate at low concentrations (Na, Al, Cl, K, Ca) must have been introduced from outside of olivine grains, and probably from dissolution of mesostasis plagioclase feldspar and apatite. The transport of Al^{3+} in solution is also consistent with acidic solutions.

Opal-A is not the only hydrous silicate present in Nakhla because Chatzitheodoridis et al. (2014) have described iron-rich saponite in the meteorite's mesostasis. They discussed several scenarios by which it may have formed, which include both abiotic water-mediated alteration and biological processes. This saponite is not juxtaposed with the Fe-Mg silicate, and so their paragenetic relationships are unknown. However, as the saponite has much higher concentrations of Al than Fe-Mg silicate (i.e., 6.3–8.8 wt% Al_2O_3 versus ~0.7 wt% Al_2O_3, respectively), the host of secondary minerals in Nakhla has clearly exerted a strong control on their chemical composition, presumably owing to low water/rock ratios (i.e., reactant compositions are controlled more by the chemistry of the hosts than by the composition of the bulk solution). It is also possible that the saponite precipitated from solutions that were less acidic than those that formed the opal-A and ferrihydrite, thus limiting the solubility and mobility of Al^{3+}. The same pattern of host mineral control on chemical compositions of secondary minerals has been found in the Lafayette nakhlite (Treiman et al. 1993; Tomkinson et al. 2013).

Formation of Siderite and its Alteration to Ferric (oxy) Hydroxide

The deuterium/hydrogen ratio of Nakhla siderite confirms its Martian origin (Saxton et al. 2000), and this carbonate would have precipitated from alkaline and reducing solutions that were rich in HCO_3, Mg, Ca, and Fe. As the pH, Eh, and chemical composition of solutions within the veins therefore changed substantially between precipitation of the opal-A plus ferrihydrite and the siderite, these iddingsite vein components are interpreted to have formed in discrete events rather than from a single evolving fluid. The conditions under which the siderite precipitated would have been conducive to replacement because in these alkaline and reducing solutions both Si and Fe^{2+} will have been soluble. The ferric (oxy)hydroxide is most likely to have formed by reaction of siderite with oxidizing Martian fluids, although as discussed above with reference to ferrihydrite shells to opal-A nanoparticles, terrestrial oxidation remains possible.

IMPLICATIONS FOR UNDERSTANDING THE PROPERTIES OF WATER WITHIN THE MARTIAN CRUST

Our finding that opal-A and ferrihydrite are together the dominant component of Nakhla iddingsite is consistent with predictions based on theoretical studies of water–rock interaction on Mars (McLennan 2003), and with results of laboratory experiments showing that aqueous alteration of terrestrial basalt under Martian conditions typically yields amorphous silica and ferric hydroxides (Baker et al. 2000; Tosca et al. 2004). It is of note that Baker et al. (2000) sought explanations for why the silica that their experiments predicted should be present within altered Martian rocks had not at that time been reported from Nakhla. The conclusions of these theoretical and experimental studies have been further validated by the discovery of extensive deposits of hydrous and amorphous opaline silica at the surface of Mars (e.g., Bandfield 2008; Mustard et al. 2008; Ehlmann et al. 2009).

The conditions under which silica forms on Mars were reviewed by Smith et al. (2013). They concluded that it will have precipitated easily and quickly during low-temperature aqueous alteration so that it cannot be used to constrain conditions of water–rock interaction (i.e., the presence of opaline silica is not diagnostic of specific fluid temperature, pressure, chemistry, etc.). Indeed the Martian deposits have diverse origins and are distributed widely; for example, (1) regional aqueous alteration in the vicinity of Valles Marineris (Milliken et al. 2008), (2) impact-induced hydrothermal alteration in Toro Crater (Marzo et al. 2010), (3) volcanically driven hydrothermal alteration in Gusev crater (Squyres et al. 2008; Ruff et al. 2011) and the Syrtis Major caldera complex (Skok et al. 2010), and (4) groundwater upwelling in Columbus crater (Wray et al. 2011). Despite opal-A having been described from only one of the nakhlites, similarities in the composition and mineralogy of iddingsite veins between Nakhla and other members of the group (Tables 1–3) suggest that amorphous and hydrous silica may have formed widely within the parent rock of these meteorites. Therefore, our work adds an Amazonian clinopyroxenite lava flow/sill to the list of Martian hosts of opaline silica, and it is notable that Syrtis Major, which hosts volcanic-hydrothermal deposits of silica, has been proposed as a source of the nakhlites (Harvey and Hamilton 2005).

We have found that the Nakhla iddingsite veins contain evidence for the former presence of several generations of aqueous solutions that had a distinctly different pH, Eh, and solute composition, although water/rock ratios are likely to have been uniformly low. The high D/H values of Fe-Mg silicate and siderite suggests that these components had formed from solutions of a similar derivation (i.e., that had equilibrated with the H-depleted Martian atmosphere), and as Fe-Mg silicate and siderite also occur together within veins from the Lafayette nakhlite (Tomkinson et al. 2013; Lee et al. 2015), these solutions were likely to have been present widely throughout the lava flow/sill. The initial fluids are interpreted to have been acidic (pH<~4) and oxidizing; they dissolved olivine and precipitated opal-A and ferrihydrite. Evidence for acidic fluids has been found at many sites on Mars, for example, via the presence of jarosite at the Opportunity landing site (Squyres et al. 2004) and ferric sulfate at Columbia Hills (Morris et al. 2006). Hurowitz et al. (2006, p. 13) concluded that acidic weathering was pervasive on Mars so that "…Martian soils represent a basaltic regolith which has undergone alteration at low pH and low water to rock ratio resulting in chemical fractionation dominated by olivine dissolution." The second pulse of solutions had a high pH and low Eh, and introduced siderite into the Nakhla veins, which formed by the replacement of olivine and the opal-A plus ferrihydrite. As the siderite often fills fractures that cross-cut the Fe-Mg silicate, it is likely that there was a considerable time gap between the first and second pulse of solutions, during which time the lava flow/sill may have experienced mild impact deformation. Evidence for the formation of siderite in the nakhlites by carbonation of silicates was first described by Tomkinson et al. (2013). The identification of this process is important for understanding the potential of carbonate precipitation to have sequestered CO_2 from the atmosphere of Mars. If these carbonates had formed by cementation, then the amount of CO_2 that could be sequestered would be limited by the porosity of the crust. However, if the carbonates formed by replacement, as suggested by Nakhla and Lafayette, then the magnitude of CO_2 drawdown would be limited only by the abundance of olivine and other components that were susceptible to carbonation (e.g., glass and An-rich plagioclase feldspar). Although comparative values for the porosity and mineralogy of the Martian crust are unavailable, it is likely that considerably more carbonate could have formed by replacement than by cementation. However, Nakhla also shows that precipitation of carbonates was not necessarily a permanent or secure means of mineralizing the Martian atmosphere because the siderite has been altered to ferric (oxy)hydroxide, with concomitant loss of CO_2.

Opal-A is unstable in terrestrial sedimentary rocks, and during diagenesis, it readily crystallizes to opal-CT, and then microcrystalline quartz by Ostwald ripening (Tosca and Knoll 2009). Thus, the ratio of opal-A to opal-CT and to quartz is a good indicator of the

longevity of liquid water within its host rock (Smith et al. 2013), and the oldest amorphous silica in Earth occurs within low permeability rocks of Cretaceous age (Tosca and Knoll 2009). Thus, the iddingsite veins provide good evidence that very little liquid water was present within the parent lava flow/sill of Nakhla after formation of the opal-A. The cristobalite and trydimite described by Thomas-Keprta et al. (2000) therefore represent the initial stages of crystallization of the amorphous silica, which may have taken place during precipitation of the siderite.

CONCLUSIONS

1. Nakhla iddingsite veins contain Fe-Mg silicate, siderite, and ferric (oxy)hydroxide. Evidence from cross-cutting relationships shows that these three components formed in that order.
2. Fe-Mg silicate is the dominant component and is composed of $\sim$12 nm diameter particles of opal-A, each of which has a shell of ferrihydrite that may also contain nontronite crystallites. This material is therefore similar in composition and microstructure to terrestrial fire opal.
3. Silicon and iron for the opal-A and ferrihydrite were sourced from the dissolution of olivine by aqueous fluids that were oxidizing and acidic. Owing to the low solubility of Si and Fe^{3+} in these solutions, the nanoparticles formed at or close to the olivine–water interface.
4. Siderite precipitated from a later pulse of reducing HCO_3-Mg-Ca-Fe solutions, and formed by the replacement of olivine and Fe-Mg silicate.
5. The final event recorded by the iddingsite veins was partial oxidation of siderite to a ferric (oxy)hydroxide, which probably took place on Mars, although a terrestrial origin cannot be discounted.
6. Solutions that formed both the opal-A plus ferrihydrite and the siderite were in equilibrium with the H-depleted Martian atmosphere, suggesting that they were sourced from near-surface reservoirs. However, the evidence for an episode of brittle deformation between formation of the Fe-Mg silicate and siderite suggests that there was a substantial time gap between the two vein components.
7. Our finding that opal-A is the main constituent of Nakhla iddingsite veins is in excellent agreement with the predictions from laboratory experiments designed to simulate aqueous alteration of the Martian crust. Spectroscopic analysis of the surface of Mars by orbiters and landers has also shown that opaline silica is widespread, and formed in a range of aqueous environments.
8. Strong similarities in chemical composition and mineralogy between Fe-Mg silicate in Nakhla and in the other nakhlites suggests that the solutions from which opal-A formed were present throughout the lava flow/sill. Further work, including quantifying variations within and between nakhlites in the size of opal-A nanoparticles, the ratios of opal-A to opal-CT and the abundance of smectite, will help to elucidate the length scale of the aqueous system and temporal and spatial variations in solution properties.
9. The preservation of opal-A nanoparticles shows that the nakhlite parent rock was exposed to little or no liquid water following formation of the iddingsite veins at $\sim$600 Ma.

Acknowledgments—The authors thank Billy Smith, Colin How, and Sam MacFadzean for help with the FIB and TEM; Peter Chung for assistance with the SEM; and the Natural History Museum (London) for loan of the Nakhla samples. The Elemental Quantification plugin used for analysis of the EELS and EDX data was provided by Dr. Paul Thomas of Gatan UK Ltd., and we are grateful for his assistance with the software. This work was funded by the UK STFC through grants ST/H002960/1, ST/K000942/1, and ST/L002167/1, and we are also grateful to SUPA and the University of Glasgow for the provision of the JEOL ARM200F. We thank Michael Velbel and an anonymous reviewer for their helpful comments on this manuscript.

Editorial Handling—Dr. Edward Scott

REFERENCES

Alexander G. B., Heston W. M., and Iler R. K. 1954. The solubility of amorphous silica in water. *The Journal of Physical Chemistry* 58:453–455.

Ashworth J. R. and Hutchison R. 1975. Water in non-carbonaceous stony meteorites. *Nature* 256:714–715.

Baker L. L., Agenbroad D. J., and Wood S. A. 2000. Experimental hydrothermal alteration of a Martian analog basalt: Implications for Martian meteorites. *Meteoritics & Planetary Science* 35:31–38.

Bandfield J. L. 2008. High-silica deposits of an aqueous origin in western Hellas Basin, Mars. *Geophysical Research Letters* 35:142–147.

Borg L. and Drake M. J. 2005. A review of meteorite evidence for the timing of magmatism and of surface or near-surface liquid water on Mars. *Journal of Geophysical Research* 110:E12S03.

Bridges J. C. and Grady M. M. 2000. Evaporite mineral assemblages in the nakhlite (Martian) meteorites. *Earth and Planetary Science Letters* 176:267–279.

Bridges J. C. and Schwenzer S. P. 2012. The nakhlite hydrothermal brine on Mars. *Earth and Planetary Science Letters* 359–360:117–123.

Bunch T. E. and Reid A. M. 1975. The nakhlites Part 1: Petrography and mineral chemistry. *Meteoritics* 10:303–315.

Burns R. G. 1991. Does Lafayette = Nakhla? Not necessarily so, based on 42K Mössbauer spectra of all the SNC meteorites (abstract). 22nd Lunar and Planetary Science Conference. pp. 157–158.

Burns R. G. and Martinez S. L. 1990. Mössbauer spectra of olivine-rich weathered achondrites: II Brachina, Chassigny, ALH 77005, and Nakhla (abstract). 21st Lunar and Planetary Science Conference. pp. 147–148.

Changela H. G. and Bridges J. C. 2011. Alteration assemblages in the nakhlites: Variation with depth on Mars. *Meteoritics & Planetary Science* 45:1847–1867.

Chatzitheodoridis E., Haigh S., and Lyon I. 2014. A conspicuous clay ovoid in Nakhla: Evidence for subsurface hydrothermal alteration on Mars with implications for astrobiology. *Astrobiology* 14:651–693.

Chevrier V., Poulet F., and Bibring J.-P. 2007. Early geochemical environment of Mars as determined from thermodynamics of phyllosilicates. *Nature* 448:60–63.

Day J. M. D., Taylor L. A., Floss C., and McSween H. Y. 2006. Petrology and chemistry of MIL 03346 and its significance in understanding the petrogenesis of nakhlites on Mars. *Meteoritics & Planetary Science* 41:581–606.

Ehlmann B. L., Mustard J. F., Swayze G. A., Clark R. N., Bishop J. L., Poulet F., Des Marais D. J., Roach L. H., Milliken R. E., Wray J. J., Barnouin-Jha O., and Murchie S. L. 2009. Identification of hydrated silicate minerals on Mars using MRO-CRISM: Geologic context near Nili Fossae and implications for aqueous alteration. *Journal of Geophysical Research* 114:E00D08.

Eugster O., Weigel A., and Polnau E. 1997. Ejection times of Martian meteotites. *Geochimica et Cosmochimica Acta* 61:2749–2757.

Friedman-Lentz R. C., Taylor G. J., and Treiman A. H. 1999. Formation of a Martian pyroxenite: A comparative study of the nakhlite meteorites and Theo's Flow. *Meteoritics & Planetary Science* 34:919–932.

Fritsch E., Gaillou E., Rondeau B., Barreau A., Albertini D., and Ostroumov M. 2006. The nanostructure of fire opal. *Journal of Non-Crystalline Solids* 352:3957–3960.

Gaillou E., Fritsch E., Aguilar-Reyes B., Rondeau B., Post J., Barreau A., and Ostroumov M. 2008. Common gem opal: An investigation of micro- to nano-structure. *American Mineralogist* 93:1865–1873.

Gillet P., Barrat J. A., Deloule E., Wadhwa M., Jambon A., Sautter V., Devouard B., Neuville D., Benzerara K., and Lesourd M. 2002. Aqueous alteration in the Northwest Africa 817 (NWA 817) Martian meteorite. *Earth and Planetary Science Letters* 203:431–444.

Gooding J. L., Wentworth S. J., and Zolensky M. E. 1991. Aqueous alteration of the Nakhla meteorite. *Meteoritics* 26:135–143.

Hallis L. J., Taylor G. J., Nagashima K., Huss G. R., Needham A. W., Franchi I. A., and Grady M. M. 2012. Hydrogen isotope analyses of alteration phases in the nakhlite Martian meteorites. *Geochimica et Cosmochimica Acta* 97:105–119.

Hallis L. J., Ishii H. A., Bradley J. P., and Taylor G. J. 2014. Transmission electron microscope analyses of alteration phases in Martian meteorite MIL 090032. *Geochimica et Cosmochimica Acta* 134:275–288.

Harvey R. P. and Hamilton V. E. 2005. Syrtis Major as the source region of the nakhlite/chassignite group of Martian meteorites: Implications for the geological history of Mars (abstract #1019). 36th Lunar and Planetary Science Conference. CD-ROM.

Hicks L. J., Bridges J. C., and Gurman S. J. 2014. Ferric saponite and serpentine in the nakhlite martian meteorites. *Geochimica et Cosmochimica Acta* 136:194–210.

Hövelmann J., Austrheim H., Beinlich A., and Munz I. A. 2011. Experimental study of the carbonation of partially serpentinized and weathered peridotites. *Geochimica et Cosmochimica Acta* 75:6760–6779.

Hurowitz J. A., McLennan S. M., Tosca N. J., Arvidson R. E., Michalski J. R., Ming D. W., Schroder C., and Squyres S. W. 2006. In situ and experimental evidence for acidic weathering of rocks and soils on Mars. *Journal of Geophysical Research-Planets* 111:E02S19.

Imae N. and Ikeda Y. 2007. Petrology of the Miller Range 03346 nakhlite in comparison with the Yamato-00593 nakhlite. *Meteoritics & Planetary Science* 42:171–184.

Imae N., Ikeda Y., Shinoda K., Kojima H., and Iwata N. 2003. Yamato nakhlites: Petrography and mineralogy. *Antarctic Meteorite Research* 16:13–33.

Janney D. E., Cowley J. M., and Buseck P. R. 2000. Transmission electron microscopy of synthetic 2- and 6-line ferryhydrite. *Clays and Clay Minerals* 48:111–119.

Karlsson H. R., Clayton R. N., Gibson E. K. Jr., and Mayeda T. K. 1992. Water in SNC meteorites: Evidence for a Martian hydrosphere. *Science* 255:1409–1411.

Kuebler K. E. 2013. A combined electron microprobe (EMP) and Raman spectroscopic study of the alteration products in Martian meteorite MIL 03346. *Journal of Geophysical Research* 118:347–368.

Lee M. R., Bland P. A., and Graham G. 2003. Preparation of TEM samples by focused ion beam (FIB) techniques: Applications to the study of clays and phyllosilicates in meteorites. *Mineralogical Magazine* 67:581–592.

Lee M. R., Brown D. J., Smith C. L., Hodson M. E., MacKenzie M., and Hellmann R. 2007. Characterisation of mineral surfaces using FIB and TEM: A case study of naturally-weathered alkali feldspars. *American Mineralogist* 92:1383–1394.

Lee M. R., Tomkinson T., Mark D. F., Stuart F. M., and Smith C. L. 2013. Evidence for silicate dissolution on Mars from the Nakhla meteorite. *Meteoritics & Planetary Science* 48:224–240.

Lee M. R., Tomkinson T., Hallis L., and Mark D. F. 2015. Formation of iddingsite veins in the Martian crust by centripetal replacement of olivine: Evidence from the nakhlite meteorite Lafayette. *Geochimica et Cosmochimica Acta* 154:49–65.

Leshin L. A., Epstein S., and Stolper E. M. 1996. Hydrogen isotope geochemistry of SNC meteorites. *Geochimica et Cosmochimica Acta* 60:2635–2650.

Lucas G., Burdet P., Cantoni M., and Hebert C. 2013. Multivariate statistical analysis as a tool for the segmentation of 3D spectral data. *Micron* 52–53:49–56.

Marzo G. A., Davila A. F., Tornabene L. L., Dohm J. M., Fairén A. G., Gross C., Kneissl T., Bishop J. L., Roush T. L., and McKay T. L. 2010. Evidence for Hesperian impact-induced hydrothermalism on Mars. *Icarus* 208:667–683.

McLennan S. M. 2003. Sedimentary silica on Mars. *Geology* 31:315–318.

Michel F. M., Barrón V., Torrent J., Morales M. P., Serna C. J., Boily J.-F., Liu Q., Ambrosini A., Cismasu A. C., and

Brown G. E. 2010. Ordered ferrimagnetic form of ferrihydrite reveals links among structure, composition, and magnetism. *Proceedings of the National Academy of Sciences* 107:2787–2792.

Mikouchi T., Miyamoto M., Koizumi E., Makishima J., and McKay G. 2006. Relative burial depths of nakhlites: An update (abstract #1865). 37th Lunar and Planetary Science Conference. CD-ROM.

Mikouchi T., Makishima J., Kurihara T., Hoffmann V. H., and Miyamoto M. 2012. Relative burial depth of nakhlites revisited (abstract #2363). 43rd Lunar and Planetary Science Conference. CD-ROM.

Milliken R. E., Swayze G. A., Arvidson R. E., Bishop J. L., Clark R. N., Ehlmann B. L., Green R. O., Grotzinger J. P., Morris R. V., Murchie S. L., Mustard J. F., and Weitz C. 2008. Opaline silica in young deposits on Mars. *Geology* 36:847–850.

Morris R. V., Klingelhofer G., Schroder C., Rodionov D. S., Yen A., Ming D. W., de Souza P. A., Fleischer I., Wdowiak T., Gellert R., Bernhardt B., Evlanov E. N., Zubkov B., Foh J., Bonnes U., Kankeleit E., Gutlich P., Renz F., Squyres S. W., and Arvidson R. E. 2006. Mössbauer mineralogy of rock, soil, and dust at Gusev crater, Mars: Spirit's journey through weakly altered olivine basalt on the plains and pervasively altered basalt in the Columbia Hills. *Journal of Geophysical Research-Planets* 111:E02S13.

Mustard J. F., Murchie S. L., Pelkey S. M., Ehlmann B. L., Milliken R. E., Grant J. A., Bibring J.-P., Poulet F., Bishop J., Dobrea E. N., Roach L., Seelos F., Arvidson R. E., Wiseman S., Green R., Hash C., Humm D., Malaret E., McGovern J. A., Seelos K., Clancy T., Clark R., Marais D. D., Izenberg N., Knudson A., Langevin Y., Martin T., McGuire P., Morris R., Robinson M., Roush T., Smith M., Swayze G., Taylor H., Titus T., and Wolff M. 2008. Hydrated silicate minerals on mars observed by the Mars reconnaissance orbiter CRISM instrument. *Nature* 454:305–309.

Needham A. W., Abel R. L., Tomkinson T., and Grady M. M. 2013. Martian subsurface fluid pathways and 3D mineralogy of the Nakhla meteorite. *Geochimica et Cosmochimica Acta* 116:96–110.

Noguchi T., Nakamura T., Misawa K., Imae N., Aoki T., and Toh S. 2009. Laihunite and jarosite in the Yamato 00 nakhlites: Alteration products on Mars? *Journal of Geophysical Research* 114:E10004.

Prior G. T. 1912. The meteoric stones of El Nakhla El Baharia. *Mineralogical Magazine* 16:274–281.

Reid A. M. and Bunch T. E. 1975. The nakhlites Part II: Where, when and how. *Meteoritics* 10:317–324.

Ruff S. W., Farmer J. D., Calvin W. M., Herkenhoff K. E., Johnson J. R., Morris R. V., Rice M. S., Arvidson R. E., Bell J. F. III, Christensen P. R., and Squyres S. W. 2011. Characteristics, distribution, origin, and significance of opaline silica observed by the Spirit rover in Gusev crater, Mars. *Journal of Geophysical Research* 116: E00F23.

Sanders J. V. 1964. Colour of precious opal. *Nature* 204:1151–1153.

Sautter V., Jambon A., and Boudouma O. 2006. Cl-amphibole in the nakhlite MIL 03346: Evidence for sediment contamination in a Martian meteorite. *Earth and Planetary Science Letters* 252:45–55.

Saxton J. M., Lyon I. C., Chatzitheodoridis A., and Turner G. 2000. Oxygen isotopic composition of carbonate in the Nakhla meteorite. *Geochimica et Cosmochimica Acta* 64:1299–1309.

Skok J. R., Mustard J. F., Ehlmann B. L., Milliken R. E., and Murchie S. L. 2010. Silica deposits in the Nili Patera caldera on the Syrtis Major volcanic complex on Mars. *Nature Geoscience* 3:838–841.

Smith M. R., Bandfield J. L., Cloutis E. A., and Rice M. S. 2013. Hydrated silica on Mars: Combined analysis with near-infrared and thermal-infrared spectroscopy. *Icarus* 223:633–648.

Squyres S. W., Grotzinger J. P., Arvidson R. E., Bell J. F. 3rd, Calvin W., Christensen P. R., Clark B. C., Crisp J. A., Farrand W. H., Herkenhoff K. E., Johnson J. R., Klingelhöfer G., Knoll A. H., McLennan S. M., McSween H. Y. Jr, Morris R. V., Rice J. W. Jr, Rieder R., and Soderblom L. A. 2004. In situ evidence for an ancient aqueous environment at Meridiani Planum, Mars. *Science* 306:1709–1714.

Squyres S. W., Arvidson R. E., Ruff S., Gellert R., Morris R. V., Ming D. W., Crumpler L., Farmer J. D., Marais D. J., Yen A., McLennan S. M., Calvin W., Bell J. F. 3rd, Clark B. C., Wang A., McCoy T. J., Schmidt M. E., and de Souza P. A. Jr. 2008. Detection of silica-rich deposits on Mars. *Science* 320:1063–1067.

Thomas-Keprta K. L., Wentworth S. J., McKay D. S., and Gibson E. K. 2000. Field emission gun scanning electron (FEGSEM) and transmisison electron (TEM) microscopy of phyllosilicates in Martian meteorites ALH 84001, Nakhla, and Shergotty (abstract #1690). 31st Lunar and Planetary Science Conference. CD-ROM.

Tomkinson T., Lee M. R., Mark D. F., and Smith C. L. 2013. Sequestration of Martian CO_2 by mineral carbonation. *Nature Communications* 4:2662.

Tomkinson T., Lee M. R., Mark D. F., Dobson K. J., and Franchi I. A. 2015. The Northwest Africa (NWA) 5790 meteorite: A mesostasis-rich nakhlite with little or no Martian aqueous alteration. *Meteoritics & Planetary Science* 50:287–304.

Tosca N. L. and Knoll A. H. 2009. Juvenile chemical sediments and the long term persistence of water at the surface of Mars. *Earth and Planetary Science Letters* 286:379–386.

Tosca N. J., McLennan S. M., Lindsley D. H., and Schoonen M. A. A. 2004. Acid-sulfate weathering of synthetic Martian basalt: The acid fog model revisited. *Journal of Geophysical Research* 109:E050003.

Treiman A. H. 2009. Martian aqueous alterations in ALH 84001 and the nakhlite meteorites (abstract #4031). Workshop on modeling Martian hydrous environments, Houston, Texas.

Treiman A. H. and Gooding J. L. 1991. Iddingside in the Nakhla meteorite: TEM study of mineralogy and texture of pre-terrestrial (Martian?) alterations. *Meteoritics* 26:402.

Treiman A. H. and Irving A. J. 2008. Petrology of Martian meteorite Northwest Africa 998. *Meteoritics & Planetary Science* 43:829–854.

Treiman A. H. and Lindstrom D. J. 1997. Trace element geochemistry of Martian iddingsite in the Lafayette meteorite. *Journal of Geophysical Research* 102:9153–9163.

Treiman A. H., Barrett R. A., and Gooding J. L. 1993. Preterrestrial aqueous alteration of the Lafayette (SNC) meteorite. *Meteoritics* 28:86–97.

Treiman A. H., Lanzirotti A., and Xirouchakia D. 2004. Synchrotron X-ray diffraction analysis of meteorites in thin section: Preliminary results (abstract #1172). 35th Lunar and Planetary Science Conference. CD-ROM.

Velbel M. A. 2009. Dissolution of olivine during natural weathering. *Geochimica et Cosmochimica Acta* 73:6098–6113.

Wray J. J., Millikeen R. E., Dundas C. M., Swayze G. A., Andrews-Hanna J. C., Baldridge A. M., Chojnacki M., Bishop J. L., Ehlmann B. L., Murchie S. L., Clark R. N., Seelos F. P., Tornabene L. L., and Squyres S. W. 2011. Columbus crater and other possible groundwater-fed paleolakes of Terra Sirenum, Mars. *Journal of Geophysical Research* 116:E01001.